ANALYSIS OF FASTENED JOINTS – PART 2: DETERMINATION OF STRESS FIELDS AROUND LOADED HOLES

Cristiano Kuchenbecker
UNESP – Escola de Engenharia de Guaratinguetá
Cristiano_kuchenbecker@hotmail.com

Carlos Eduardo Chaves
EMBRAER – Empresa Brasileira de Aeronáutica S/A
Carlos.chaves@embraer.com.br

Fernando de Azevedo Silva
UNESP – Escola de Engenharia de Guaratinguetá
Fazevedo@feg.unesp.br

Abstract. *In this paper, detailed analyses based on the finite element method (FEM), are performed for a typical butt joint configuration of an aircraft fuselage. The following items are evaluated: (a) elements used for skin representation, where plate and solid elements are considered; (b) elements used for rivets representation, where the importance of bending and shear forces is discussed; (c) elements used to represent the transmission between plates and rivets (rigid and interpolation elements, solid elements) and the necessity of applying such elements in the general context; (d) improvements that are obtained by applying contact between two plates and between plates and rivets. Results of analysis taking into account each of these items are presented.The analytical results are compared to strain fields obtained by photoelasticity.*

Keywords*. Butt joints, finite element method, stress concentration factors, photoelasticity*

1. Introduction

During aircraft design practice, one could consider in general two scenarios for analysis of fastened (or riveted) joints: the first one is a fastened joint as a part of a substructure, where obviously the level of detail must be reduced due to the magnitude of the region being analyzed, and where the major concerns will be a somehow qualitative understanding of the average stress increases due to these geometric discontinuities and the amount of load that is transferred to each row of fasteners. Such approach was discussed in the first part of this investigation, where strains obtained by strain gages located far from the rivet holes were measured and compared with values obtained from the numerical model. The model was based on plate elements for the skin representation and beam elements to simulate the rivets.

The second scenario could be thought as a detailed evaluation of stress fields for typical joint configurations over the aircraft, where the boundary conditions would be obtained from locations near the joint and only a small region representing each joint type would be used for the analysis. The purpose of this second evaluation is to obtain with a reasonable degree of accuracy the magnification of stresses around the fastener holes and consequently to compute stress concentration factors (Kt's), allowing better means for prediction of crack initiation due to cyclic fatigue loads in such components.

This work, which is complementary to Part 1 of the investigation, has two main objectives. The first one is to obtain reasonable results by applying linear elastic analysis. In Part 1, it was shown that, mainly for lap joints, the eccentricity between plates causes the so-called secondary bending, and that such bending is clearly a nonlinear response of the structure. However, as long as the numerical model becomes more detailed, nonlinear analysis becomes prohibitive, and it is naturally desirable to perform linear analysis. The second objective is to show the influence of elements used for rivet simulation and connections between rivets and plates in the stress and strain fields around the fastener hole, and to accomplish this many detailed models will be used.

The experimental procedure adopted for validation of the numerical models was the photoelasticity, such that some details about the photoelastic procedure and results obtained from the experiment will be also briefly discussed.

2. Experimental Procedure

Photoelasticity is one of the most usual procedures to measure stress fields due to singularities. Many stress concentration factors available in classical handbooks, such as the Peterson's Compilation of Stress Concentration Factors (Pilkey, 1997) relied on this experimental method prior to numerical methods available nowadays.

There are many specific references about photoelasticity, and sections about photoelastic analysis (and other experimental methods for stress and strain measurement) are often found in structural analysis books. The book of Redner and co-workers (Redner et. al., 1977) presents a good overview of the subject. For a photoelastic test, initially it is necessary to attach a photoelastic coat into the surface to be analyzed. The coat has a reflective material such that when the plate is polarized the light is reflected. When the returning light passes through appropriated filter lens, it is possible to identify the so-called *isoclinic* fringes (regions where all principal stresses have the same direction) and *isochromatic* fringes (regions where it is possible to measure differences between principal stresses). Figure 1 shows the

testing machine that was used for the photoelastic evaluation and the polarized light reflecting into the photoelastic plates. As it can be seen from this figure, the rivet heads are not covered by the photoelastic coat, once they are slightly out of the skin outer planes and the stress values over the rivet heads should not be measured.

There are many aspects regarding coat sensitivity that should be observed for selection of the appropriate photoelastic coat thickness. A more detailed discussion about coat thickness and many considerations for testpiece preparation for photoelastic analysis with fastened joints can be found in recent work of Kuckenbecker (2002).

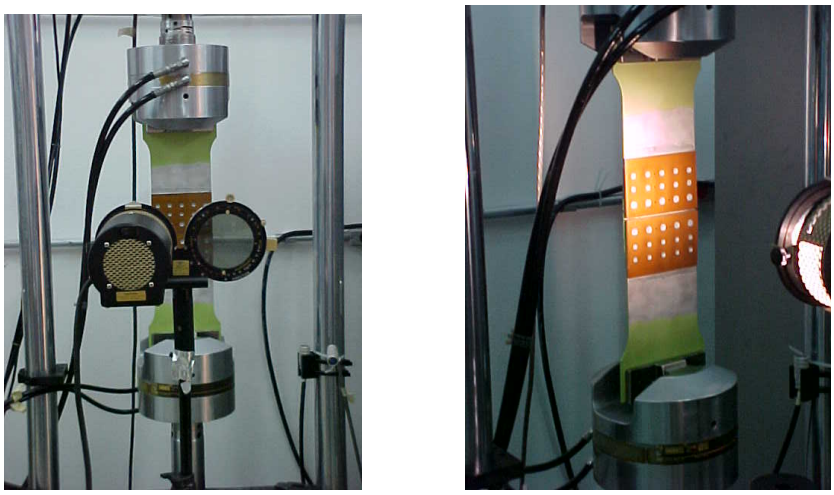

Figure 1. Testpiece and test apparatus for photoelastic analysis in a fastened joint.

A universal tensile machine MTS-810 series was used for this experiment. The test was performed at the Embraer Structural Test Laboratory facilities. The quasi-static load was applied until a maximum value of 36000 N was reached.

The photoelastic analysis allows to obtain qualitative results by means of the isochromatic fringes as well as (quantitative) punctual values. For the present investigation, initially some points along the skin surface where chosen for verification of strain values over the butt joint connections, as shown in Figure 2, where points 1, 2, 3 and 4 are expected to have nearly the same stress values, due to symmetry. Then the testpiece is subjected to tensile load and the isoclinics are measured in order to obtain the principal stress angles at these points. Once these angles are known, the isoclinics are then removed by changing the polariscope lens and the isochromatic fringes are visualized as shown in Figure 3. The number of fringes increases as long as the load level increases and according to the photoelastic coat thickness limitations.

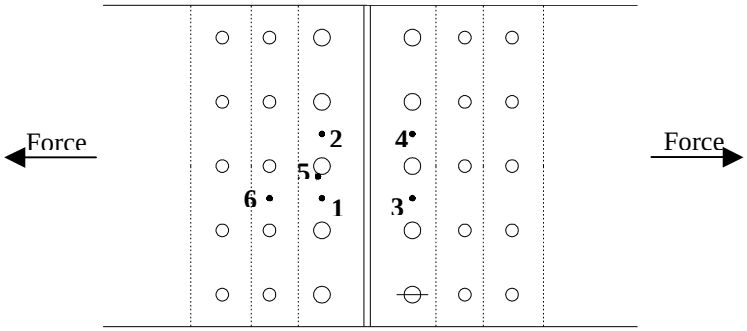

Figure 2. Points selected for strain measurement.

Figure 3. Isochromatic fringes for the fastened butt joint.

The punctual strain values are obtained according to a photoelastic equation, as follows:

$$\varepsilon_1 - \varepsilon_2 = N.\frac{\lambda}{2.t_c.K} \tag{1}$$

Where ε_1 and ε_2 are the principal strains (maximum and minimum), N is the fringe number, obtained according to the load level, λ is the polariscope light wave length (22,7 x 10^{-6} in), t_c is photoelastic plate thickness (0.081 in in this case) and K is the sensibility factor, that is available from the photoelastic plate coat manufacturer. The maximum shear strain is given by:

$$\frac{\gamma_{máx}}{2} = \frac{\varepsilon_1 - \varepsilon_2}{2} \tag{2}$$

Such that the maximum shear strain is obtained from the above equations as follows:

$$\gamma_{máx} = \varepsilon_1 - \varepsilon_2 = N.\frac{\lambda}{2.t_c.K} \tag{3}$$

The values obtained for points 1, 5 and 6 are presented in Table 1. The results for points 2, 3 and 4 were as expected similar to the ones observed for point 1. These values will be used for comparison with the finite element models to be described in the following section.

Table 1 – Strain results obtained from photoelastic analysis for points 1, 5 and 6.

Point	Strain	Maximum shear stress ($\gamma_{máz}$) [MPa]
1	0.00148	39.5
5	0.00175	46.7
6	0.00171	21.0

3. Finite Element Analysis

The fastened joint that was used for this analysis is a tapered joint with three rows of rivets at each side, whose plates are made of Al-7475-T7351 (Modulus of Elasticity E = 70000 MPa and Poisson Ratio ν = 0.33) and the fasteners are made of Titanium for aerospace applications (Modulus of Elasticity E = 116000 MPa and Poisson Ratio ν = 0.33). Figure 4 shows the outline and dimensions of the testpiece that was later used for all models.

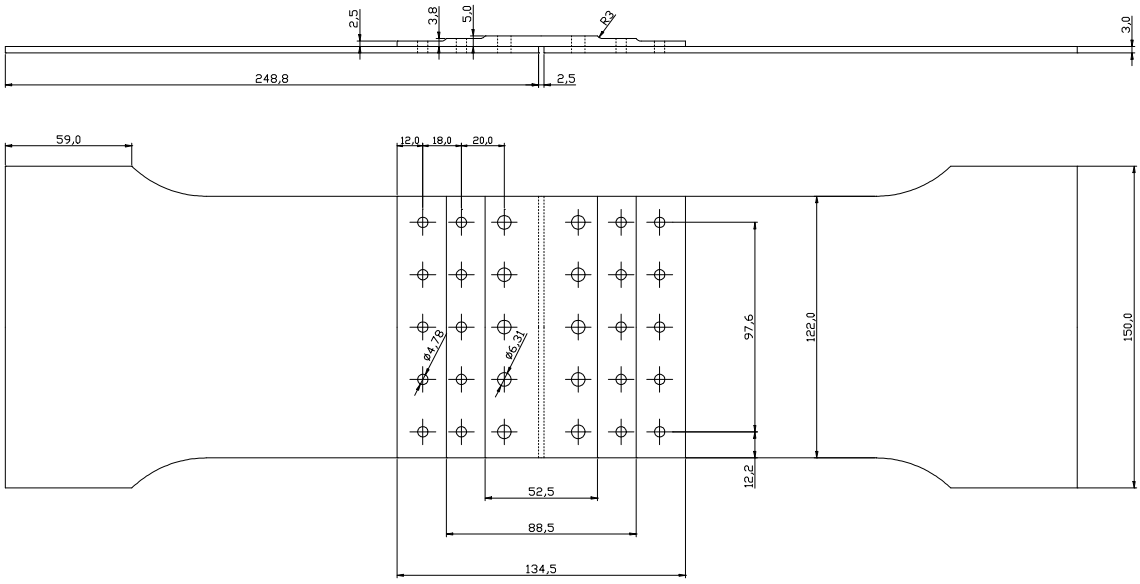

Figure 4. Outline and main dimensions of the specimen used for photoelastic evaluation and numeric analysis.

In contrast with the lap joint configuration, the butt joint presents a symmetry plan at the middle line of the strap, and such characteristic allows that for all models a symmetry plan is used for this region. For the specimen edge, the applied boundary condition was such that only translation along the longitudinal direction was allowed and the applied load was equal to the maximum value measured during the experiment (36000 N). Further, the connection between plate and load application point for the testpiece was simulated by means of rigid elements (RBE2). Once again, symmetry plans along the longitudinal direction were avoided for this configuration because of the rivets that must be sectioned along the symmetry plans.

3.1. Analysis with plate elements

All the analyses were carried out with the MSC.Nastran V.2001 finite element analysis solver. Initially, two models were developed with plate elements CQUAD4 (with 24 degrees of freedom and linear interpolation) and CQUAD8 (with 64 degrees of freedom and parabolic interpolation).

In a preliminary analysis, no connection elements were used to simulate rivet heads, and the skin plate elements were directly connected to the rivet uni-dimensional elements. Due to the differences in plate thickness for the strap for each row of rivets, element *offsets* were used. Figure 5(a) shows the outline of these models with plate elements. The plate width-to-thickness ratios are generally high (close to 5) although the element transverse shear property was applied, allowing smaller ratios with very accurate results. Additionally, plate models where the connection between plates and rivets was taken into account were developed. For these models, the level of refinement was higher and many configurations for the connecting elements were tested. The detail of the rivet region for these models is shown in Figure 5(b).

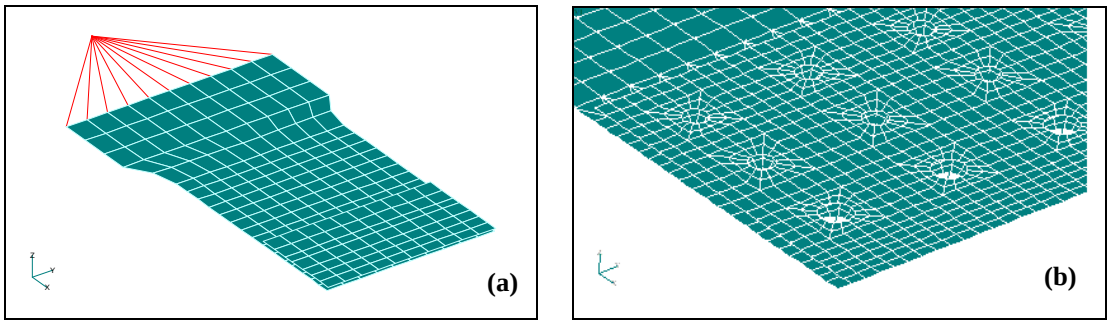

Figure 5. Outline of finite element models with plate elements (a) without connection elements and (b) with connection elements at the rivet holes.

The fastener elements were simulated as simple beam elements (BAR Element, according to MSC.Nastran nomenclature) aiming to support the joint shear and bending stiffness, coupled with scalar spring elements (CELAS), intended to support bearing stiffness. The beam element properties require some adjust in the flexibility based on semi-empirical data, described in Part 1 of this work and whose background is found in the work of Swift (1971), while the spring element property is set according to the spring stiffness by the relation:

$$K = \frac{1}{F} \tag{4}$$

where F is the transverse flexibility, that will be the same as the one obtained for the beam element. For the configuration being evaluated, each fastener row has different geometry characteristics, such that the spring stiffness values used for the analysis were 76923 MPa, 69091 MPa and 66667 MPa for the first, second and third rows of rivets respectively. Figure 6 shows a schematic representation of the deformed rivet (excluding bending effects). This proposed configuration (BAR + CELAS) is based on experimental observation of strain fields in a specimen (experiment described in the first part of this investigation) and lacks of rigorous theoretical basis, although it shows successful for a wide range of loads applied in the joint. A similar proposal, although much more difficult to implement, is found in the work of Rutman et. al (1999).

The connection elements between skin and strap plates and the rivets were simulated in six different manners, and such comparison was carried out for plate elements and solid elements to be described in the following section. The configurations evaluated were: (1) rigid connections (RBE2) all around the rivet holes; (2) rigid connections (RBE2) for one half of the rivet holes, somehow simulating a contact condition; (3) connections through interpolation elements (RBE3) all around the rivet holes; (4) connections through interpolation elements for one half of the rivet holes; (5) connections through interpolation elements with varying weight all around the rivet holes and (6) connections through interpolation elements with varying weight for one half of the rivet holes. While rigid connections may be easy to understand, the concept of interpolation element is less intuitive. Such element (RBE3) transfers the load through the

structure uniformly, and the resulting displacement will be averaged and computed for the load application point. The weight function allows that the amount of load that is transferred changes from node to node, simulating for example a sinusoidal load, that is what occurs for a contact problem.

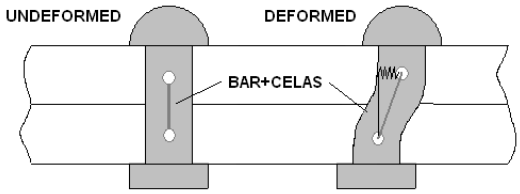

Figure 6. Schematic representation of fastener BAR+CELAS modeling.

3.2. Analysis with solid elements

In a second step, solid elements were used to simulate the plates. Figure 7(a) shows an outline of the model region close to the rivet holes. The plates and straps were simulated with four layers of HEXA4 elements (hexahedron elements with linear interpolation). The connections between solid elements and rivet elements were performed in six different manners, as previously explained, and Figure 7(b) shows a detail of the connection region. The elements represented in red in this figure may be rigid (RBE2) or interpolation (RBE3) elements, according to the case analyzed.

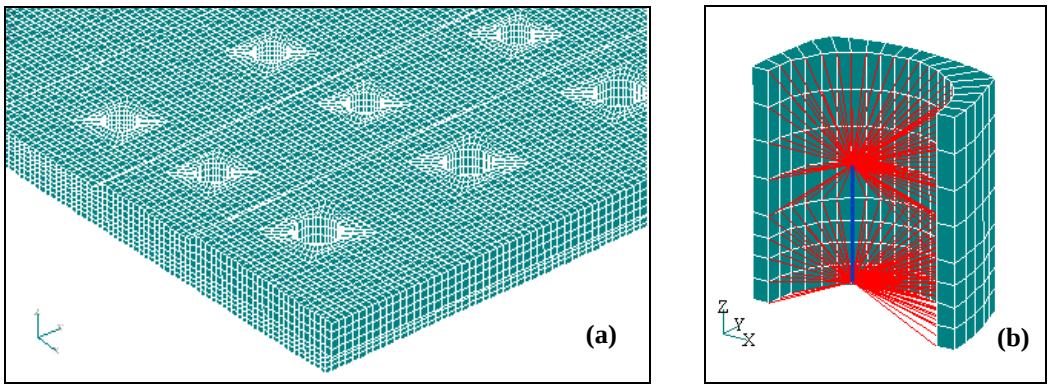

Figure 7. Model with solid elements: (a) region close to rivet connections; (b) detail of rivet connection.

In a third step, with solid elements being used to simulate the plates, such elements were also used to simulate the rivets, and contact analysis was performed between plate and plate (skin and strap) and plates and rivets. The contact algorithm used for this analysis was the so-called *linear GAP* element available in Nastran solver, which is a series of multi-point constraint (MPC) equations which, by means of an iterative solver, are able to simulate nonlinearities of contact phenomena. Details of the contact analysis will not be presented in this paper, but may be found in recent work of Kuchenbecker (2002) or in MSC.Nastran software documentation.

The solid elements show some advantages and drawbacks when compared to the plate elements previously described. They do not require a orientation and do not have width-to-thickness constraints, but in contrast they require that a certain number of elements (four in the present case) are put through the plate thickness and the models usually become time-consuming due to the large number of degrees of freedom.

4. Results and Discussion

The scenario of a deformed joint with regions of stress concentration is shown schematically in Figure 8. There will be stress concentrations due to shear forces, secondary bending and also due to bearing forces from the rivets. This complex interaction of concentration effects will be only represented appropriately if contact effects are accounted for. However, many difficulties arise for application of contact in a finite element model. Contact is highly non-linear, such that the analysis becomes time consuming and not necessarily converges. As a matter of fact, the model with linear gap elements that was developed for this study comprises only three rivets. A full model was tested at Embraer CAE facilities and even with plenty of resources available it was not possible to run such model presently, due to the excessive size of temporary files created to solve contact equations.

Nevertheless, the purpose here is to find a suitable model for an accurate evaluation of stress concentration effects. Ideally, a global-local model could be used, and the results here presented would be the ones obtained from the local model. With respect to the other configurations analyzed, they will be much useful for future evaluations once such

models show that they represent the stress fields appropriately if compared to the very refined model with contact analysis, assumed to be the most representative.

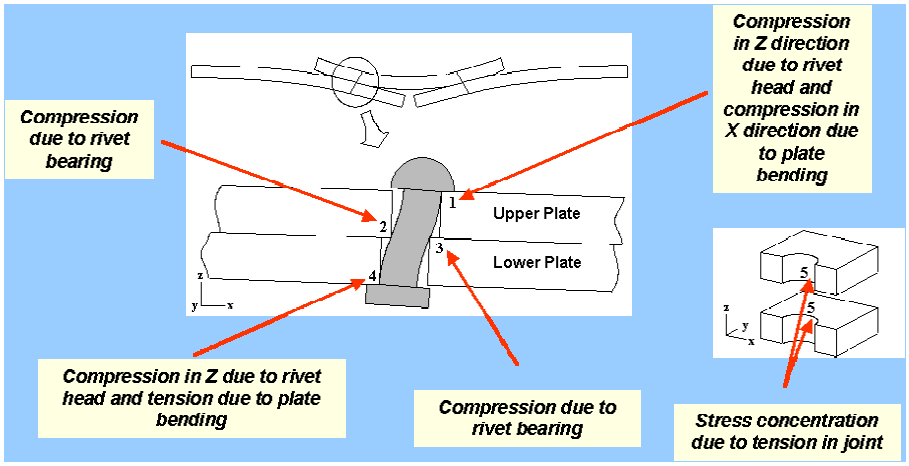

Figure 8. Loads and stress concentrations for the riveted joint.

The summary of strains measured in points No. 1, No. 5 and No. 6 (see Figure 2) for the most important models among all the plate and solid models developed for this work is shown in Table 2. The results from photoelasticity are shown in the first line. Changes in results due to the type of element (QUAD4, QUAD8 or HEXA8) and due to the connection used (RBE2 and RBE3) are shown in the table. The results from the model with contact are not included in this table, because as mentioned before this model includes only three rivets from one row and there will be differences due to symmetry effects in the boundaries.

The models with solid elements present higher strain values when compared to models with plate elements. That is because apparently plate elements (with coarser meshes) tend to reduce corner stresses and strains when recovering corner data to (average) element data. The plate model with QUAD8 elements (elements with parabolic interpolation) seems to have a good agreement with photoelasticity results. Among the models with solid elements, the one with interpolation elements (RBE3) with varying weight function all around the rivet hole seems to be the one with the closest results if compared to photoelasticity.

Figure 9, in the following page, shows the outline of the deformed models for all solid configurations, except the one from contact analysis and the one with interpolation elements (RBE3) with varying weight function for half of the rivet hole. Results for the upper plate (splice) and lower plate (skin) from the detail in the box (inner row of rivets) are shown separately. Stress values in the legend are in daN/mm^2 (or in 1/10 of MPa) It is interesting to compare the stress concentration points with the regions where the largest stress concentrations are expected according to the concepts presented in Figure 8.

Selected results from the contact model analysis are presented in Figures 10 and 11. Figure 10 shows qualitatively the Von Mises stress fringes for this model, separating the upper and lower stress fields that are obtained for the upper and lower plates. The largest stress value is in the lower part of the upper plate (strap) and that is likely to be a crack initiation point. It should be noted that the rivet heads are not modeled, and perhaps they would exert influence in the stress concentrations. A model with contact and including the rivet heads is left as a suggestion for future studies. Figure 11(a) shows the regions with more concentration for compression or tension stresses and in the *x* and *z* directions. It is interesting again to compare these results with concentration points 1 to 4 in Figure 8 above. Figure 11(b) shows the deformed model, where there are regions with contacting surfaces and other with free surfaces according to what is expected from the study presented in Figure 8.

Table 2. Results for the main models selected from the analysis, comparison with photoelasticity

Models	Strain at point No. 1	Strain at point No. 5	Strain at point No. 6
Photoelasticity	0,00148	0,00175	0,00171
CQUAD4 - without rivet hole connections	0,00077	---	0,00120
CQUAD8 - without rivet hole connections	0,00078	---	0,00128
CQUAD8 - with rivet hole connections	0,00066	0,00174	0,00133
HEXA8 - RBE2 all around the rivet holes	0,00131	0,00320	0,00250
HEXA8 - RBE2 in half of the rivet holes	0,00120	0,00930	0,00270
HEXA8 - RBE3 with unit weight all around the rivet hole	0,00120	0,00290	0,00268
HEXA8 - RBE3 with unit weight for half of the rivet hole	0,00122	0,00590	0,00280
HEXA8 - RBE3 with varying weight all around the rivet hole	0,00121	0,00265	0,00269
HEXA8 - RBE3 with varying weight for half of the rivet hole	0,00126	0,00400	0,00283

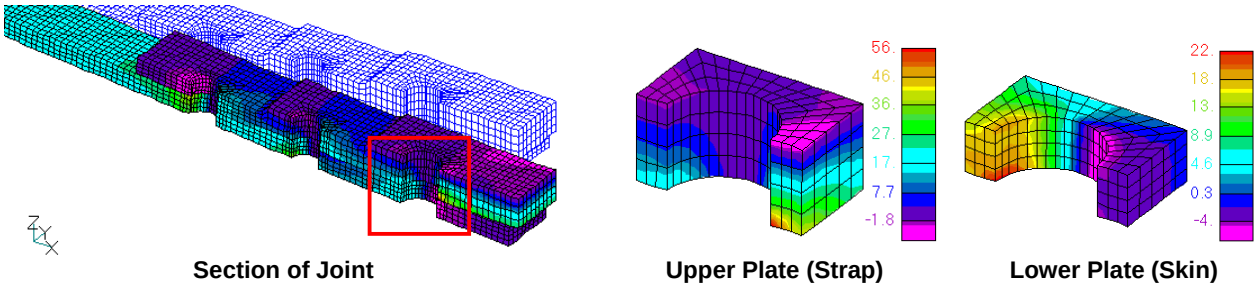

Section of Joint | Upper Plate (Strap) | Lower Plate (Skin)

RIGID CONNECTIONS (RBE2) ALL AROUND THE RIVET HOLES

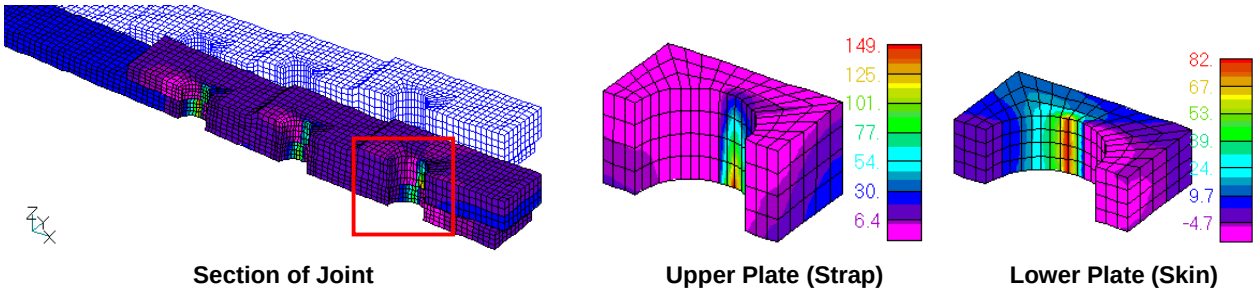

Section of Joint | Upper Plate (Strap) | Lower Plate (Skin)

RIGID CONNECTIONS (RBE2) HALF OF THE RIVET HOLES

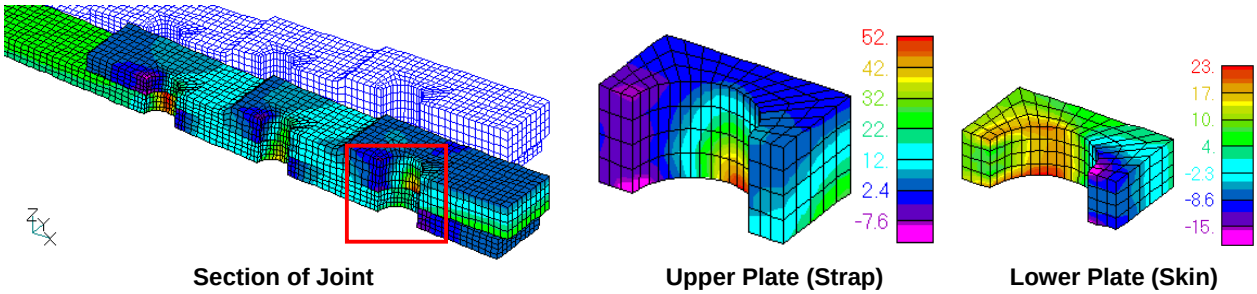

Section of Joint | Upper Plate (Strap) | Lower Plate (Skin)

INTERPOLATION CONNECTIONS (RBE3) ALL AROUND THE RIVET HOLES

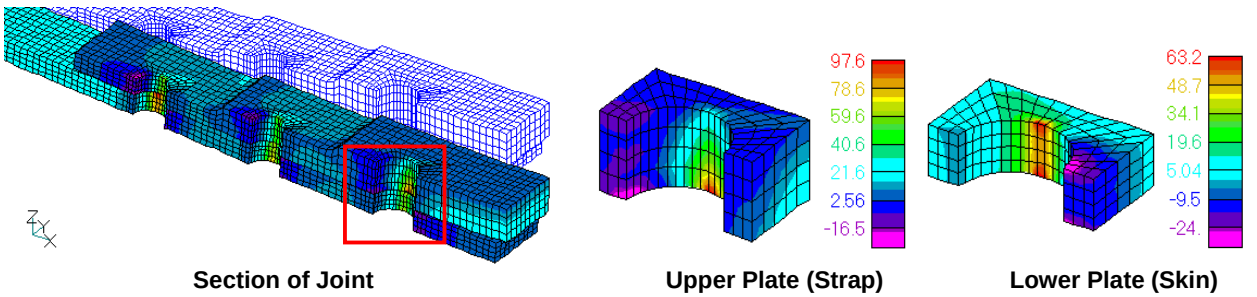

Section of Joint | Upper Plate (Strap) | Lower Plate (Skin)

INTERPOLATION CONNECTIONS (RBE3) HALF OF THE RIVET HOLES

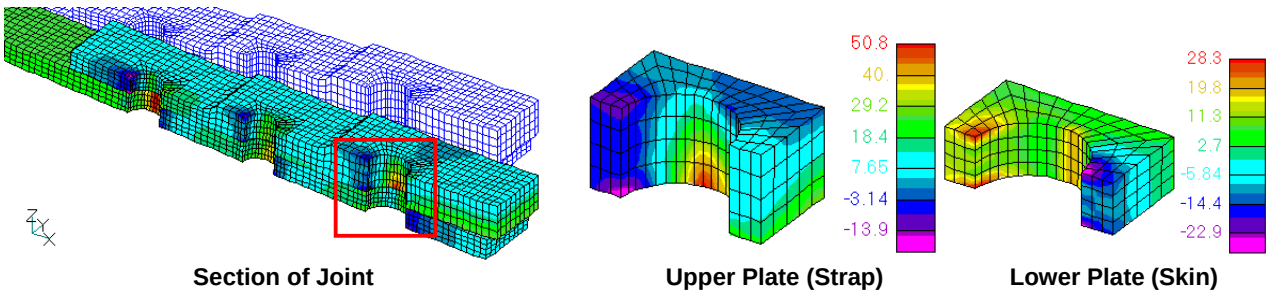

Section of Joint | Upper Plate (Strap) | Lower Plate (Skin)

INTERPOLATION CONNECTIONS (RBE3) ALL AROUND RIVET HOLES WITH WEIGHT FUNCTION

Figure 9. Deformed and contour results for the solid configurations analyzed (except contact).

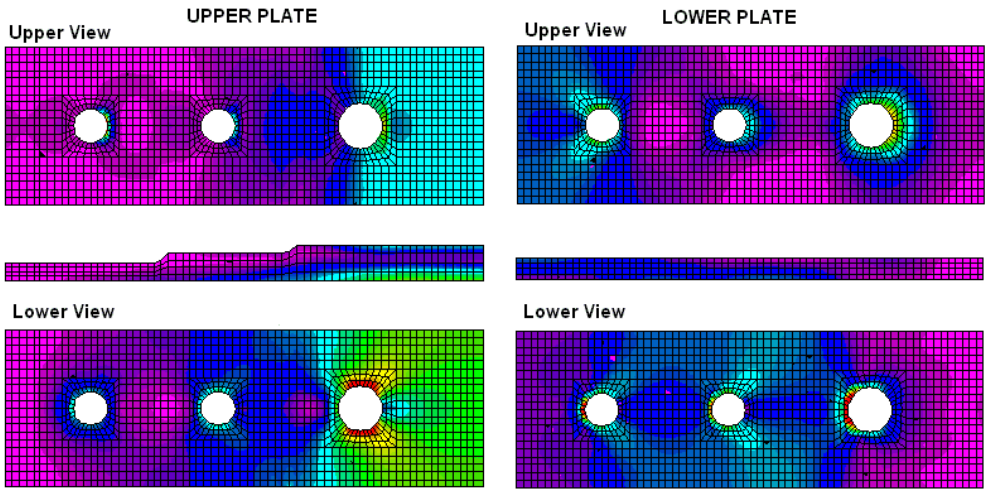

Figure 10. Outline of Von Mises stress fields for model with contact.

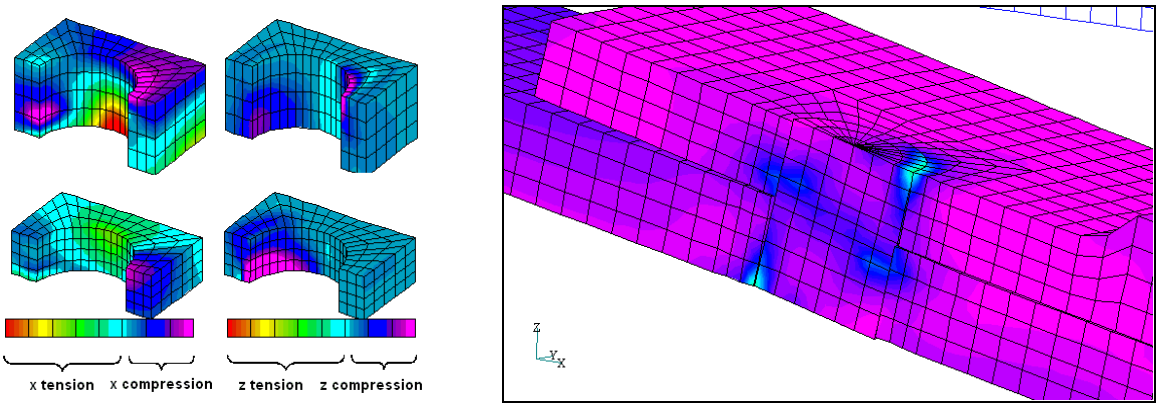

Figure 11. Deformed model with stress concentration regions obtained from contact analysis.

Figure 12 below presents qualitatively the comparison between the FEM model results and the photoelastic stress fringes for a set of three rivets (each one in a different row) in the specimen central region. While the fringes clearly show differences close to the border, once as previously explained the model is limited to a strip of three rivets only, there is a reasonable agreement for fringes close to the hole borders.

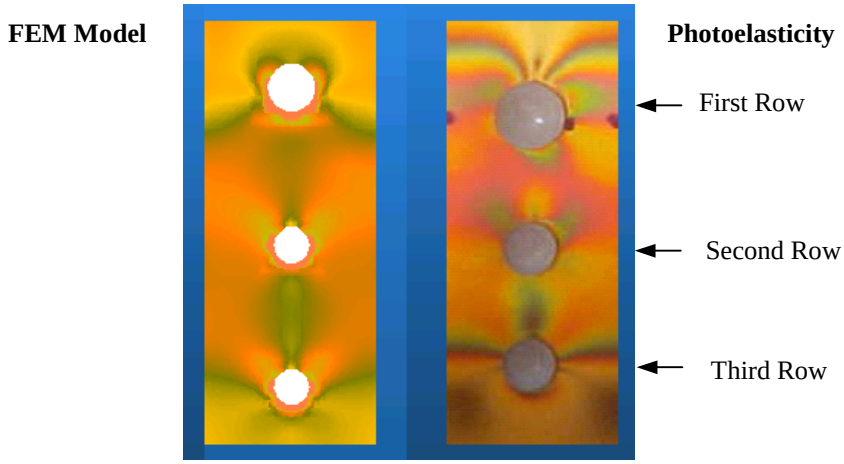

Figure 12. Comparison between photoelastic fringes and FEM results obtained from model with contact.

5. Conclusions

A series of refined finite element models with plate and solid elements were analyzed and results from three points along the joint and close to the rivet positions were compared with the ones obtained with photoelastic measurements. For the evaluation of stress fields and stress concentration factors, the model accounting for contact between plates and between plates and rivets is the most appropriate. However, models with solid elements for the plates, uni-directional beam and spring elements for the rivets and interpolation elements for the connections between plates and rivets also presented good agreement with the experiment.

Among the plate elements analyzed, the results showed that CQUAD8 elements with rivet hole connections should be used for such analysis.

For solid elements, although the last option (HEXA8 - RBE3 model with varying weight for half of the rivet hole) presented strain levels higher than the corresponding values obtained from photoelasticity, this model showed the closest results if compared to the photoelastic results and also showed the best agreement if compared to the solid model with contact. Therefore such configuration is recommended for detailed analysis in joints.

6. References

Redner, S., Zandman, F., Dally, J. W., “Photoelastic Coatings”, Society for Experimental Stress Analysis, 1977.

Pilkey, W.D. “Peterson’s Stress Concentration Factors” – Second Edition, 1997.

Kuchenbecker, C. “Avaliação de Modelos Placa-Sólido Para Juntas Rebitadas Utilizando o Método dos Elementos Finitos”, Graduation Thesis, 2002.

Swift, T. “Development of the Fail-Safe Design Feature of the DC-10”, Damage Tolerance in Aircraft Structures, ASTM STP 486, American Society for Testing and Materials, 1971.

Rutman, A., Bales-Kogan, J., “Multi-Spring Representation of Fasteners for MSC.Nastran Modeling”, MSC Aerospace Conference, 1999.